Supplement of

Cold-stage system for Impact-initiated Contact freezing Experiments (C-ICE)

Jingchuan Chen[1], Upasna B. Rai[1], Kyle A. McMillan[2,3], Ryan D. Davis[4,5], Margaret A. Tolbert[2,3], and Sarah D. Brooks[1*]

[1] Department of Atmospheric Sciences, Texas A&M University, College Station, Texas 77843, USA
[2] Cooperative Institute for Research in Environmental Sciences, University of Colorado, Boulder, Boulder, Colorado 80309, USA
[3] Department of Chemistry, University of Colorado, Boulder, Boulder, Colorado 80309, USA
[4] Sandia National Laboratories, Albuquerque, New Mexico 87123, USA
[5] Department of Chemistry and Chemical Biology, University of New Mexico, Albuquerque, New Mexico 87131, USA

Correspondence to: Sarah D. Brooks (sbrooks@tamu.edu)

This file includes:

Figures S1 to S6;

Tables S1 to S4; and

Movie S1 (available from the Texas Data Repository at https://doi.org/10.18738/T8/4LM3BB).

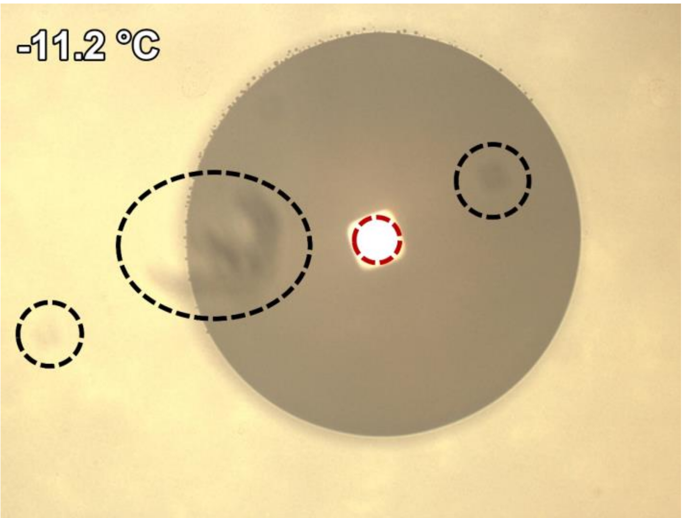

Figure S1. Illustration of the image region used for grayscale analysis, shown using the optical image acquired at -11.2 ℃ as an example. The region enclosed by the red dashed circle at the center of the droplet was used to calculate the grayscale value, from which the time series shown in Fig. 2a was derived. The irregular patterns highlighted by the black dashed circles are stationary optical artefacts originating from imperfections on the microscope optical path. These features remained fixed throughout all experiments, appeared consistently in every image, and were excluded from the analysis. Consequently, they do not affect the grayscale calculations, freezing detection, or any results presented in this study.

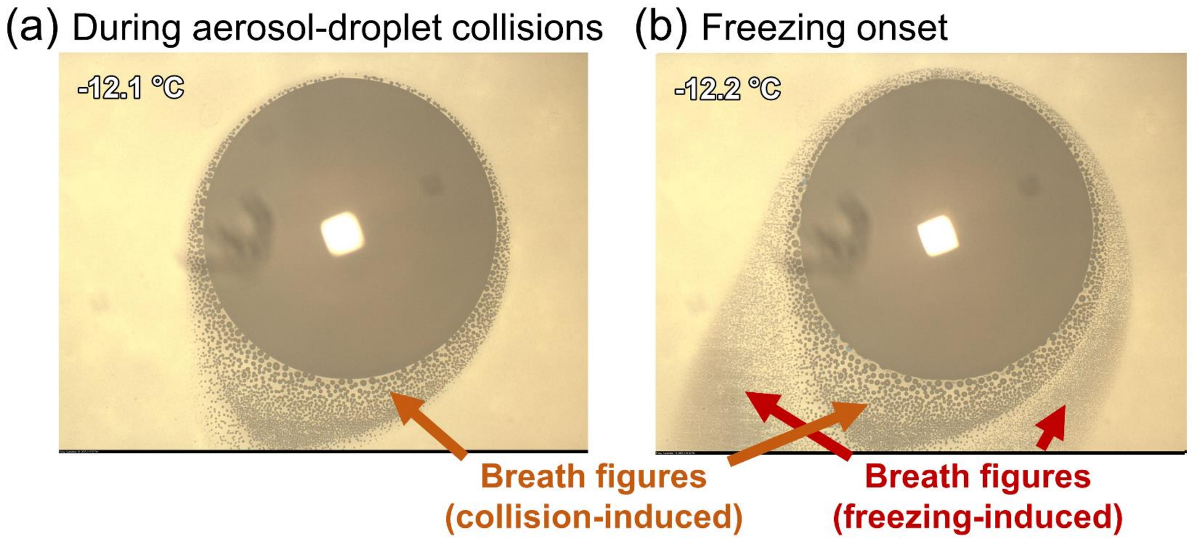

Figure S2. Comparison of breath figure formation immediately (a) before and (b) at the onset of impact-initiated contact freezing. (a) A supercooled droplet during aerosol-droplet collisions at -12.1 ℃, approximately 0.1 ℃ above the onset freezing temperature. Localized breath figures are present in the droplet wake region due to collision-induced vapor saturation, but no freezing-induced condensation pattern is observed. (b) The same droplet at the onset freezing temperature (-12.2 ℃). In addition to the collision-induced breath figures, a distinct condensation ring appears around the droplet perimeter as a result of latent heat release associated with the initiation of freezing. The appearance of this secondary breath-figure pattern provides a robust optical indicator of freezing onset and distinguishes freezing-induced condensation from background vapor-field effects during aerosol-droplet interactions.

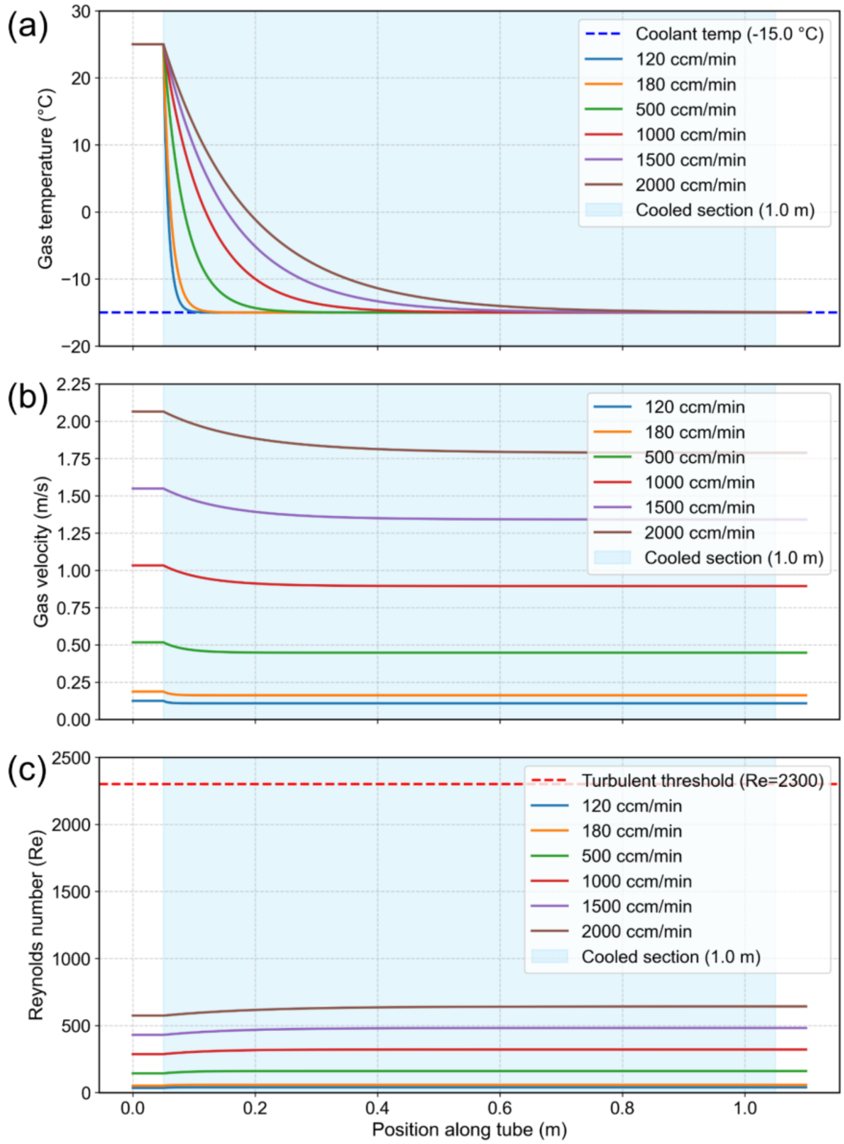

Figure S3. Simulated axial evolution of gas temperature, flow velocity, and Reynolds number in the dehumidifier section of the C-ICE system under different flow rates. (a) Gas temperature profiles along the dehumidifier tube for flow rates ranging from 120 to 2000 cm^3 min^{-1}, with the coolant temperature fixed at -15 °C (dashed blue line). (b) Corresponding axial profiles of gas velocity for the same flow conditions. (c) Reynolds number (Re) as a function of axial position, with the turbulent transition threshold (Re = 2300) indicated by the dashed red line. The shaded light blue region in all panels denotes the cooled section of the dehumidifier (length = 1.0 m), where the particle-laden airstream flows through the inner tube of the concentric heat-exchange assembly. For all investigated flow rates, the flow remains well within the laminar regime throughout the cooled section.

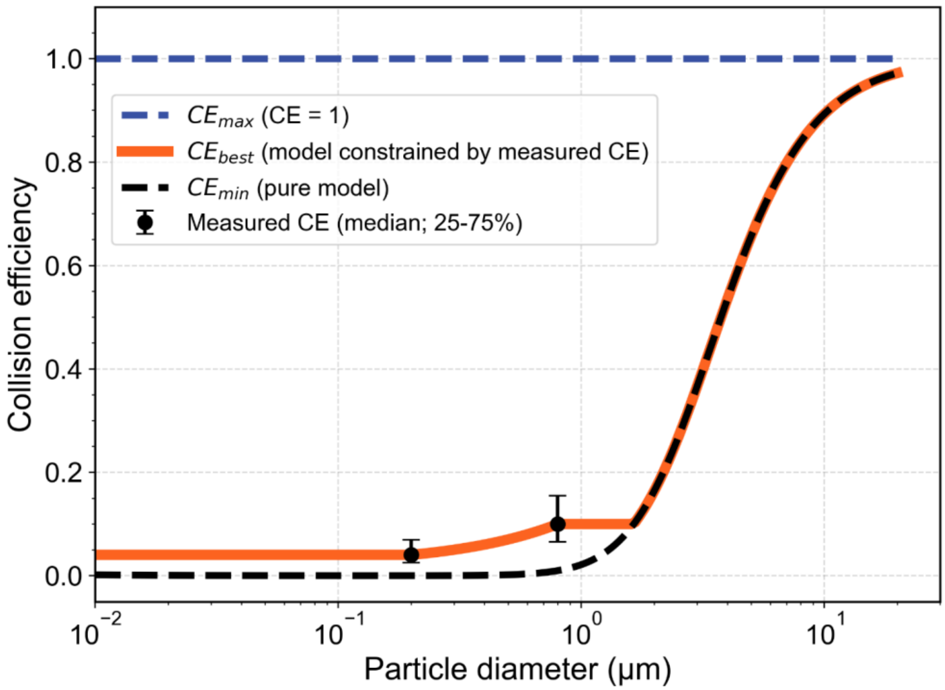

Figure S4. Experimentally constrained collision efficiency for the C-ICE system. The same datasets and model curves as in Fig. 6 are shown, but plotted on a linear y-axis. The linear scale highlights the absolute magnitude of collision efficiencies at small particle diameters.

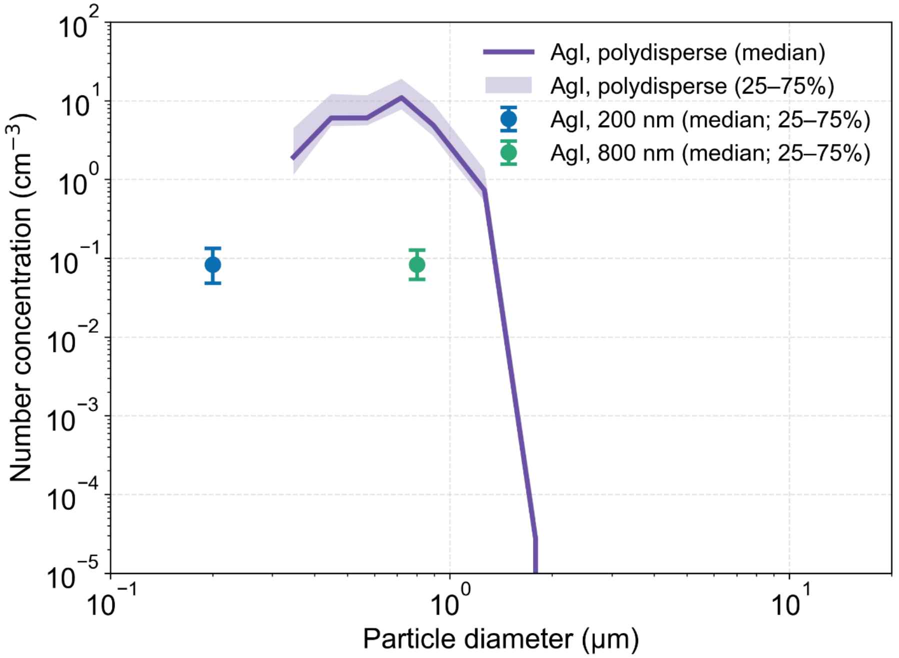

Figure S5. Particle number concentrations as a function of particle diameter for AgI aerosols used in the C-ICE experiments. Results are shown for the polydisperse AgI aerosol (median with interquartile range, 25-75%; obtained from an optical particle counter, OPC), together with number concentrations for monodisperse 200 nm and 800 nm AgI particles (median; 25-75%; obtained from a condensation particle counter, CPC). The same datasets as in Fig. 7b are used, but expressed here as number concentration (cm^{-3}). Multiplication of the number concentrations by the experimental flow rate yields the effective particle collision rates shown in Fig. 7b.

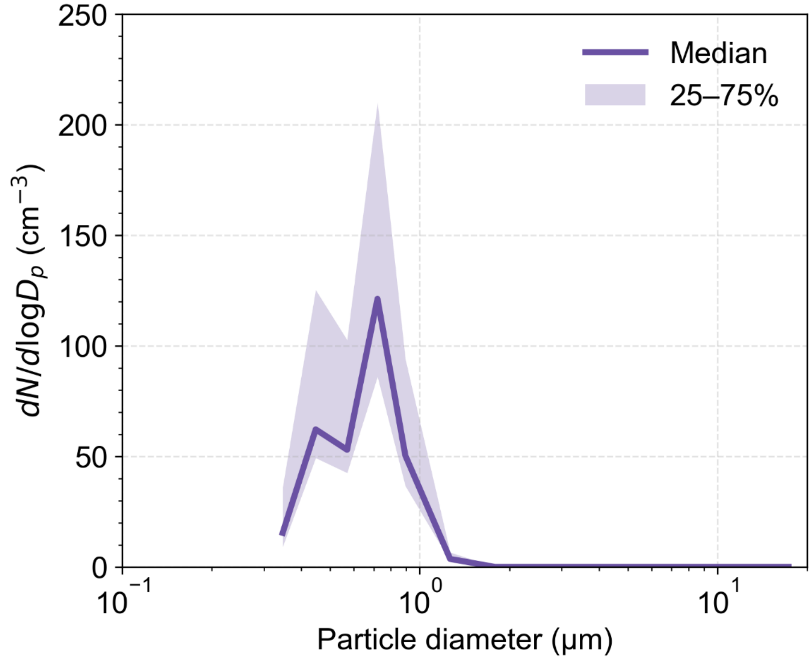

Figure S6. Particle number size distribution of the polydisperse AgI aerosol. The median distribution (solid purple line) and the interquartile range (25-75%, shaded area) are shown. The distribution, measured using an OPC, is used to weight size-dependent collision efficiencies in the calculation of effective particle collision rates shown in Fig. 7b.

Table S1. Statistical summary of characteristic freezing temperatures for impact-initiated contact freezing experiments under different aerosol conditions. The onset and complete freezing temperatures are reported for monodisperse AgI particles (200 nm and 800 nm), polydisperse AgI particles, and the particle-free background. For each case, the 25th percentile (25%), median, 75th percentile (75%), mean, standard deviation (STD), the total number of freezing events (n), and median freezing temperature (T_{50}) are listed. Across all AgI-containing cases, the difference between onset and complete freezing temperatures is consistently within 0.2-0.3 ℃, while the particle-free background exhibits substantially lower freezing temperatures and larger variability. Note that the reported T_{50} was defined as the temperature at which $f_{ice}(T) = 0.5$. Therefore, the value may differ slightly from the median of the measured freezing temperatures due to discretization and interpolation, typically by 0.1 ℃.

Characteristic freezing temperature (℃)	200 nm		800 nm		Polydisperse		Particle-free background
	Onset	Complete	Onset	Complete	Onset	Complete	
25%	-12.3	-12.5	-11.9	-12.1	-9.8	-10.0	-26.3
Median	-12.7	-12.9	-12.1	-12.3	-10.2	-10.4	-28.7
75%	-13.1	-13.3	-12.3	-12.5	-10.6	-10.9	-30.2
Mean	-12.7	-12.9	-12.1	-12.3	-10.2	-10.4	-28.8
STD	0.5	0.5	0.3	0.3	0.5	0.5	2.6
T_{50}	-12.6	-12.8	-12.0	-12.2	-10.1	-10.4	-28.8
n	31		34		50		21

Table S2. Experimentally inferred collision efficiencies ($\mathrm{CE_{exp}}$) for 200 nm and 800 nm AgI particles in impact-initiated contact freezing experiments. For each particle size, the 25th percentile (25%), median, 75th percentile (75%), mean, and the total number of evaluated events (n) are reported. The values of n differ from those listed in Table S1 because $\mathrm{CE_{exp}}$ can only be derived for freezing events with concurrent and reliable aerosol number concentration measurements from CPC and/or OPC instruments. Consequently, only a subset of the total freezing events contributes to the collision efficiency statistics.

$\mathrm{CE_{exp}}$	200 nm	800 nm
25%	0.03	0.07
Median	0.04	0.10
75%	0.07	0.15
Mean	0.05	0.11
n	29	32

Table S3. Statistical summary of effective particle collision rates (s^{-1}) for 200 nm and 800 nm AgI particles in the C-ICE experiments, corresponding to Fig. 7b. Particle rates were derived from experimentally constrained collision efficiencies combined with measured aerosol number concentrations under the experimental flow conditions. Reported values include the 25th percentile (25%), median, 75th percentile (75%), and mean. The sample size n reflects the number of events with valid collision efficiency and particle concentration measurements.

Effective particle collision rate (s^{-1})	200 nm	800 nm
25%	0.10	0.11
Median	0.17	0.17
75%	0.27	0.26
Mean	0.20	0.29
n	29	32

Table S4. Summary statistics of particle number concentrations for AgI aerosols used in the C-ICE experiments. Number concentrations are reported for monodisperse 200 nm and 800 nm AgI particles as well as for the polydisperse AgI aerosol, corresponding to the distributions shown in Figs. S5 and S6. Values are presented as the 25th percentile (25%), median, 75th percentile (75%), mean, and the total number of events (n).

Number concentration (cm^{-3})	200 nm	800 nm	Polydisperse
25%	0.05	0.05	22.22
Median	0.08	0.08	31.82
75%	0.13	0.13	56.74
Mean	0.10	0.15	51.45
n	29	32	47

Movie S1. Visualization of an impact-initiated contact freezing experiment using 200 nm AgI particles, corresponding to the case shown in Fig. 2. The movie shows the evolution of the droplet during the freezing process together with the corresponding temperatures. The movie is available from the Texas Data Repository at https://doi.org/10.18738/T8/4LM3BB. Key stages of the droplet state and freezing process are summarized below.

Temperature (℃)	Droplet state and process description
-11.2	Supercooled liquid droplet
-11.4	Supercooled liquid droplet; onset of aerosol-droplet collisions
-11.8	Supercooled liquid droplet; during aerosol-droplet collisions
-12.2	Onset of contact freezing
-12.4	Fully frozen droplet (ice phase)